Protective coatings for intraocular wirelessly controlled microrobots for implantation: Corrosion, cell culture, andin vivoanimal tests

Pokki, Juho ; Ergeneman, Olgaç ; Chatzipirpiridis, George ; Lühmann, Tessa ; Sort, Jordi ; Pellicer, Eva ; Pot, Simon A ; Spiess, Bernhard M ; Pané, Salvador ; Nelson, Bradley J

Abstract: Diseases in the ocular posterior segment are a leading cause of blindness. The surgical skills required to treat them are at the limits of human manipulation ability, and involve the risk of permanent retinal damage. Instrument tethering and design limit accessibility within the eye. Wireless microrobots suturelessly injected into the posterior segment, steered using magnetic manipulation are proposed for procedures involving implantation. Biocompatibility is a prerequisite for these procedures. This article investigates the use of polypyrrole- and gold-coated cobalt-nickel microrobots. While gold has been used in ocular implants, no ocular implantation involving polypyrrole is reported, despite its well-established biocompatibility properties. Coated and uncoated microrobots were investigated for their corrosion properties, and solutions that had contained coated and uncoated microrobots for one week were tested for cytotoxicity by monitoring NIH3T3 cell viability. None of the microrobots showed significant corrosion currents and corrosion potentials were as expected in relation to the intrinsic nobility of the materials. NIH3T3 cell viability was not affected by the release medium, in which coated/uncoated microrobots were stored. In vivo tests inside rabbit eyes were performed using coated microrobots. There were no significant inflammatory responses during the first week after injection. An inflammatory response detected after 2 weeks was likely due to a lack of longer-duration biocompatibility. The results provide valuable information for those who work on implant technology and biocompatibility. Coated microrobots have the potential to facilitate a new generation of surgical treatments, diagnostics and drug-delivery techniques, when implantation in the ocular posterior segment will be possible.

DOI: https://doi.org/10.1002/jbm.b.33618

Society For Biomaterials

Protective coatings for intraocular wirelessly controlled microrobots for implantation: Corrosion, cell culture, and *in vivo* animal tests

AQ5 Juho Pokki,[1] Olgaç Ergeneman,[1] George Chatzipirpiridis,[1] Tessa Lühmann,[2] Jordi Sort,[3] Eva Pellicer,[4] Simon A. Pot,[5] Bernhard M. Spiess,[5] Salvador Pané,[1] Bradley J. Nelson[1]

[1]Institute of Robotics and Intelligent Systems, ETH Zurich, CH-8092 Zurich, Switzerland
[2]Institute for Pharmacy and Food Chemistry, University of Würzburg, DE-97070 Würzburg, Germany
[3]Institució Catalana de Recerca i Estudis Avançats (ICREA) and Departament de Física, Universitat Autònoma de Barcelona, E-08193 Bellaterra, Spain
[4]Departament de Física, Universitat Autònoma de Barcelona, E-08193 Bellaterra, Spain
[5]Equine Department, Vetsuisse Faculty, University of Zurich, CH-8057 Zurich, Switzerland

Received 21 July 2015; revised 22 November 2015; accepted 3 January 2016
Published online 00 Month 2016 in Wiley Online Library (wileyonlinelibrary.com). DOI: 10.1002/jbm.b.33618

Abstract: Diseases in the ocular posterior segment are a leading cause of blindness. The surgical skills required to treat them are at the limits of human manipulation ability, and involve the risk of permanent retinal damage. Instrument tethering and design limit accessibility within the eye. Wireless microrobots sutureless injected into the posterior segment, steered using magnetic manipulation are proposed for procedures involving implantation. Biocompatibility is a prerequisite for these procedures. This article investigates the use of polypyrrole- and gold-coated cobalt-nickel microrobots. While gold has been used in ocular implants, no ocular implantation involving polypyrrole is reported, despite its well-established biocompatibility properties. Coated and uncoated microrobots were investigated for their corrosion properties, and solutions that had contained coated and uncoated microrobots for one week were tested for cytotoxicity by monitoring NIH3T3 cell viability. None of the microrobots showed significant corrosion currents and corrosion potentials were as expected in relation to the intrinsic nobility of the materials. NIH3T3 cell viability was not affected by the release medium, in which coated/uncoated microrobots were stored. *In vivo* tests inside rabbit eyes were performed using coated microrobots. There were no significant inflammatory responses during the first week after injection. An inflammatory response detected after 2 weeks was likely due to a lack of longer-duration biocompatibility. The results provide valuable information for those who work on implant technology and biocompatibility. Coated microrobots have the potential to facilitate a new generation of surgical treatments, diagnostics and drug-delivery techniques, when implantation in the ocular posterior segment will be possible. J Biomed Mater Res Part B: Appl Biomater 00B: 000–000, 2016.

Key Words: ophthalmic microrobots; biocompatibility; corrosion; cell culture; rabbit model

How to cite this article: Pokki J, Ergeneman Oç, Chatzipirpiridis G, Lühmann T, Sort J, Pellicer E, Pot SA, Spiess BM, Pané S, Nelson BJ. 2016. Protective coatings for intraocular wirelessly controlled microrobots for implantation: Corrosion, cell culture, and *in vivo* animal tests. J Biomed Mater Res Part B 2015:00B:000–000.

INTRODUCTION

Diseases in the posterior segment of the eye, such as age-related macular degeneration and diabetic retinopathy, affect the ocular function of over 8 million people in the USA alone.[1,2] These disorders are the most common causes leading to permanent vision loss in the industrialized countries. They are currently treated with instruments that require the visual and tactile perception of a surgeon. The surgical skills required are at the limits of human capabilities, and many retinal treatments risk permanent damage to the retina. Furthermore, accessibility within the eye is limited by instrument tethering and design.[3–5] Minimally invasive, wirelessly controlled and powered microrobots[6] are alternatives proposed for use in ocular medicine. Injected sutureless into the eye[5] [Figure 1(A, B)], they can be precisely steered with 5 degrees of freedom using external magnetic fields generated by a magnetic manipulation system.[4] The system controls the forces and torques that the microrobot applies during surgery, and the microrobot's location is tracked visually through the pupil. The microrobot can precisely access regions of the eye that conventional tools cannot reach. F1

Several potential ophthalmic applications, such as fluorescent dye-based oxygen sensing[7] for diagnosis of retinal hypoxia, retinal vein puncturing[8,9] for precisely targeted injections, intravitreal micromechanical measurements,[10] and drug delivery[11,12] for retinal diseases, have been demonstrated using microrobots. Unlike conventional ophthalmic drug-delivery procedures (i.e., with tablets, eye drops, and lotions) that must be administered

Correspondence to: J. Pokki; e-mail: jpokki@ethz.chor S. Pané i Vidal; e-mail: vidalp@ethz.ch
AQ2 Contract grant sponsor: European Research Council Advanced Grant BOTMED

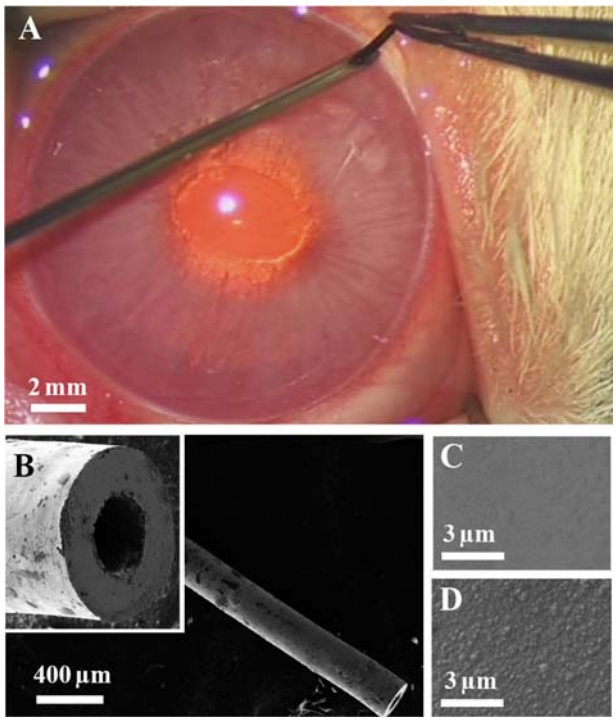

COLOR

FIGURE 1. **A**: A Ppy-coated microrobot to be injected suturelessly via a 23G needle into a living rabbit eye. The microrobot is loaded into the needle using suture forceps with flat tying platform. The photograph is rotated and mirrored for clarity. **B**: The SEM image shows a typical cylindrical CoNi microrobot as prepared. The inset shows a magnified detail of one end. Microrobots were coated with Au and with Ppy, which are shown in the following SEM images. **C**: Au coating on the surface of a CoNi microrobot. **D**: Ppy coating prepared on a Au-coated microrobot. Imaging was carried out using a Zeiss Ultra 55.

frequently to maintain the required therapeutically relevant tissue levels of the drugs, implantable steerable microrobots offer an alternative strategy as therapeutic reservoirs. Drugs can be released directly to the target during an extended period while minimizing possible side effects to surrounding tissues. The drug can be encapsulated[9,11] inside the microrobot or included on a multi-layered functional surface.[12]

In ophthalmic applications, the microrobot can be implanted in the posterior segment of the eye in the proximity of ocular structures needing treatment/diagnosis. A targeted drug-delivery[4,11,12] application to treat age-related macular degeneration requires implantation. Vessel-targeted injections with thrombolytics for central retinal artery and vein occlusions are further potential applications. The microrobots can be steered and oriented during a procedure using a magnetic manipulation system[4] designed for the microrobots. They can be implanted in a desired location. After implantation the microrobots can be controllably retrieved from the eye[5] using the same manipulation system. The system is capable to align them with and maneuver them toward a custom-made "reverse" injector with a magnetic shaft,[5] and the shaft can be used to pull the microrobot inside the injector. A critical factor for the success of these new therapies is the biocompatibility of the microrobots, which is a function of shape, size, the physical, chemical and surface properties of the used materials, the interaction of the microrobots with specific regions of the eye, the presence of an ocular immune response, and duration of the interaction.

Progress on ocular biomaterial research is demonstrated by the widespread use of contact lenses, and the frequent use of intraocular lenses implanted in cataract surgeries. This has spurred research on biomaterials for implantable devices such as glaucoma filtration devices, scleral buckles, and keratoprostheses. In contrast, research on biomaterials for the posterior segment is still in early development as posterior segment implants themselves are a relatively new phenomenon.[13] Several metals and polymers are used as an implant material and as an implant coating.

The typical metals used in ophthalmic surgery instruments are titanium and stainless steel, because their acute ocular toxicity is negligible.[14] Additionally, new suturing techniques in anterior segment surgery have used nitinol intraocular clips that have not demonstrated any short-term toxicity in mini-pig eyes.[15] Titanium tacks have exhibited long-term biocompatibility in rabbit eyes and may provide a permanent and stable option for anchoring intraocular implants in the posterior segment.[16] In several medical applications, titanium coating provides superior surface adhesion properties and microsurface smoothness *in vitro* and *in vivo*.[16] However, functionalization of these metals can be challenging.

Gold[17,18] (Au) is a good candidate for ocular implant coatings due to its nobility, inert nature, resistance against bacterial colonization, as well as its potential functionalizability. Used also as an adhesion layer, Au enables further electrodeposition of other functional coatings.

Two types of polymer materials, erodible and nonerodible, have been used in intraocular implants that are already on the market or close to commercialization. One of the most long-standing implants, Ozurdex,[19] consists almost entirely of bioerodible poly(lactide-*co*-glycolide) (PLGA). Although the by-products of bioerosion (water and carbon dioxide) are nontoxic, acidification during degradation is detrimental for biological function (i.e., protein delivery). The Retisert[20] implant, approved by the FDA for treating uveitis, is composed of a combination of nondegradable poly(vinyl alcohol) (PVA) and nonerodible silicone elastomer held together by silicone glue. The Retisert implant therefore has to be surgically retrieved after implantation. Iluvien is a another nondegradable insert made from poly(imide) with PVA caps to control the rate of drug release[21] and is in clinical use to treat diabetic macular edema.

New, better tunable and functionalizable polymers are needed for future ocular applications. Polypyrrole (Ppy) has well-established long-term biocompatibility with a variety of cell types (e.g., as neural prosthetics[22]). It is the best-characterized intrinsically conducting polymer due to its versatile and tunable properties, and also exhibits mechanical stability and ease of synthesis. Ppy can be prepared as a conformal functional coating onto microstructures of different shapes. Its surface properties can be electrochemically tuned due to its property of redox switching.[23]

In this article, cylindrical microrobots made of magnetic cobalt-nickel (CoNi) alloy (allowing magnetic manipulation), coated with Au and Ppy, are explored for their biocompatibility

TABLE I. Four Different Types of Microrobot Surfaces Prepared.

Types	Surface
Uncoated	Electroformed CoNi
Au type I	Electrolessly deposited Au
Au type II	Electrodeposited Au
Ppy	Electrodeposited Ppy

in ocular applications. The corrosion performance of the coated (Au and Ppy) and uncoated microrobots (as-prepared CoNi) is investigated. Hank's balanced salt solution (HBSS) was used for modeling the corrosion properties of the vitreous to mimic its primary component. HBSS is a standard physiological solution, used as anterior eye chamber fluid replacement, as intraocular irrigation fluid and a typical model used in ophthalmic toxicology studies.[24] *In vitro* cell viability as determined by cell proliferation of NIH3T3 fibroblasts was performed to investigate potential release of metal ions or leachables from coated and uncoated microrobots for implantation after 1 week of storage in solution. Finally, *in vivo* trials with coated microrobots [Figure 1(A, B)] were carried out inside the eyes of living New Zealand white rabbits with a follow-up of 49 days.

MATERIALS AND METHODS

Fabrication of the microrobots

The fabrication of tubular microrobots [Figure 1(B)] is described in detail elsewhere.[9] The outer diameter (OD) of all the microrobots was restricted to 300 ± 10 μm to satisfy the size requirements of the inner diameter (ID) of the 23G needle used for sutureless injection into the ocular vitreous. Solid CoNi microrobots were fabricated on a Au wire (250 μm in diameter) to provide the electrical connection required in the electrochemical corrosion tests. Cell tests were carried out with similar microrobots. A CoNi layer 25 μm thick was deposited on the wire to obtain the final OD of 300 μm. For *in vivo* studies, the microrobots were fabricated on a thinner sacrificial aluminum wire (125 μm in diameter; pre-coated with 0.2-μm-thick Au in bright electroless Au bath at 90°C for 12 min, Transene company, Danvers, MA). The thinner wire allowed for preparation of sufficient magnetic material (CoNi) for magnetic manipulation. Hence, CoNi 88 μm thick was electroformed on the wire to obtain the final OD of 300 μm. Subsequently, the aluminum wire was etched, and only the electrolessly prepared Au coating remained covering the hollow interior of the microrobot. Microrobots were then coated for the tests. Their surface after coating with Au and Ppy is shown in Figure 1(C, D), respectively.

Preparation of the coatings

Prepared as shown in Table I, solid microrobots without coating (controls) and with coatings from two different materials (Au and Ppy) (Figure 2), were used in corrosion and in cell tests. The microrobots used *in vivo* had their outer surface coated with Ppy and their inner surface coated with Au (i.e., hollow interior used as a potential drug reservoir). The same coating methods were used as with the solid microrobots. The Au layer serving as a potential final coating or as an adhesive layer for further coatings was prepared using two methods. Au coating type I was prepared by electroless deposition by immersing an implant into a bright electroless Au bath (from Transene company, Danvers, MA) at 90°C for 12 min. Au coating type II [Figure 1(C)] was prepared by electrodeposition in a Au bath with a formulation described by Jang et al.[25] Both types, 0.2-μm-thick coatings, were compared in corrosion and in cell tests. The use of Au enabled subsequent electrodeposition of Ppy on the CoNi microrobots.

Ppy [Figure 1(D)] was galvanostatically electropolymerized on the Au-coated microrobots. In preparing the Ppy coating,[23] an electroplating bath containing 0.1 M sodium dodecylbenzene sulfonate (NaDBS) and 0.1 M pyrrole was used. A current density of 1 $mA \cdot cm^{-2}$ was applied on the microrobot for 10 min to get a thickness of approximately 3 μm. The microrobot served as the working electrode (WE) and a platinum-coated titanium plate as the counter electrode (CE), together with a reference electrode (RE). A double junction Ag|AgCl RE was used with 3 M KCl inner solution and a 0.1 M NaDBS outer solution.

The microrobots with Ppy surfaces were cathodically doped to gain antibiofouling[23] properties for the cell and for the *in vivo* tests. Cathodic doping was performed in a 0.1 M NaDBS aqueous solution with the same electrode arrangement employed in the Ppy electropolymerization. The doping was carried out by cyclic voltammetry (3 cycles; scan rate of 10 $mV \cdot s^{-1}$) between 0 V and −0.7 V.

Corrosion tests

HBSS (Sigma, H8264-500 mL) was used to evaluate the corrosion properties of the microrobots' materials and coatings. The electrochemical cell equipment used for the corrosion tests is presented in Supporting Information (Figure S1). The cell filled with 100 mL of HBSS was thermostated at body temperature (37°C). Each microrobot was immersed 2 mm into the HBSS using a micropositioner (SmarAct GmbH, HCU-3D). Three electrodes were immersed into the HBSS (WE, CE, and RE). The microrobot was used as the WE. A platinum-coated helical titanium wire was used as the CE for applying a homogeneous electric field around the microrobot (see Supporting Information Figure S1). The RE

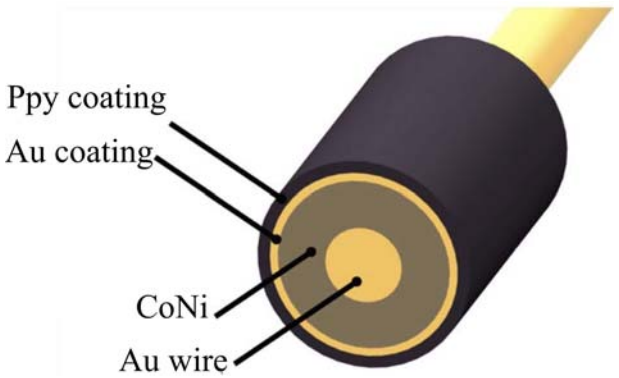

COLOR

FIGURE 2. The cross-sectional view of a solid microrobot, that is, coated with Au and Ppy.

was a double-bridge (Ag | AgCl (3 M KCl)) filled with HBSS in the outer bridge. The samples were subject to an open-circuit potential (OCP) for 5 h in order to determine the steady-state potential. Then, potentiodynamic polarization tests were performed by scanning at a scan rate of 0.1 $mV \cdot s^{-1}$ from 300 mV below the obtained OC*P* value toward more positive values up to 300 mV above the OCP. Between three and six replicas per microrobot type were tested. A paired *t* test with Bonferroni correction for the comparison of multiple groups was used to validate the significance (95% confidence level) of the differences between the microrobot types regarding their corrosion potential. The specimens were subjected to SEM imaging (Merlin Zeiss), energy dispersive X-ray (EDX) and X-ray photoelectron spectroscopy (XPS) analysis after the corrosion tests. XPS analyses were carried out on a PHI 5500 Multitechnique System (from Physical Electronics) spectrometer, equipped with a monochromatic X-ray source ($K_{\alpha Al}$ line with energy of 1486.6 eV and 350 W).

Fibroblast proliferation assay

Prior to the experiments, the microrobots (Figure 2) were sanitized for >12 h in 70% ethanol and were washed three times with phosphate buffered saline (PBS) containing 1% Penicillin/Streptomycin antibiotics (Biochrom A2212) in an Eppendorf tube. They were stored in 400 μL of PBS containing 1% Penicillin/Streptomycin as a release medium for one week at room temperature. NIH3T3 fibroblasts (ATCC-Number CRL-1658, ATCC, Manassas, VA), harvested from subconfluent monolayers, were incubated in 25 cm^2 culture flasks at 37°C and 5% CO_2. The growth medium (DMEM) included 10% heat-inactivated fetal bovine serum (Invitrogen 10270) and 1% Penicillin/Streptomycin. NIH3T3 fibroblast proliferation was characterized by the mitochondrial activity of living cells using a tetrazolium dye (MTT) based colorimetric assay as previously described in Sivaraman et al.[23] 5000 fibroblast cells were seeded in 100 μL growth medium in a 96-well plate. On the next day 100 μL of PBS, in which the different types of microrobots had been stored for 7 days, was added for 24 h prior to analysis. The cell proliferation was then normalized with the mitochondrial activity of the cells cultured in pure PBS with 1% Penicillin/Streptomycin (i.e., control). A minimum of four samples was used for *in vitro* cell experiments. The MTT assay is a common and standard assay to assess cell proliferation as readout for toxicity and is routinely performed with antibiotics in the test medium.[23,26] Although it is generally possible to perform the assay without antibiotics, they were used in the first toxicity screening for monitoring potential adverse effects of the microrobots reported here. The control group was therefore treated similarly with PBS containing 1% antibiotics and set to 100% viability.

***In vivo* rabbit experiments**

The microrobots were washed in an acetone bath, then in an isopropanol-ethanol (1:1) solution and finally in DI water prior to injecting into the *in vivo* rabbit eyes (healthy New Zealand white rabbits, 9 month-old female). The microrobots were subsequently autoclave sterilized. Prior to the injection the rabbits were anesthetized. Animal housing, anesthetic and surgical procedures, and post-procedure examinations were performed in laboratory animal facilities at the Vetsuisse Faculty, University of Zurich.

Two groups of rabbits were used (Groups A and B) with six individuals in each group. The rabbits in Group A, received a microrobot injected into a randomly assigned eye (referred to as Group A1). The fellow eyes of these rabbits served as internal controls (referred to as Group A0). Group B served as control group for the microrobot injections. Rabbits in Group B received a sham injection into a randomly assigned eye (referred to as Group B1). The fellow eyes of these rabbits served as internal controls (referred to as Group B0).

Sutureless injections into the rabbit eyes were carried out via a standard 23G needle through the pars plana of the ciliary body into the vitreous (see Figure 3). Successful injections into the right eye were performed at the 10–11 o'clock position and into the left eye at the 1–2 o'clock position. The maximum distance between the injection site and internal limbus observed during injection was 1 mm. Preliminary *ex vivo* injection experiments in rabbit eyes obtained from slaughter demonstrated this distance as optimal to ensure safe insertion of the microrobots into the central vitreous while avoiding damage to critical tissues (e.g., lens and retina). In Group A1, the microrobots were injected using 0.1 mL hyaluronic acid (HA, Acrivet Biovisc 1.2%), which helped to push the robot away from the needle tip. For each rabbit receiving an intravitreal microrobot, there was a control rabbit (Group B1) that received a sham-injection of 0.1 mL HA only, which was identical in all aspects other than the insertion of a microrobot. The noninjected eyes (i.e., fellow eyes) of the rabbits served as internal controls (Groups A0 and B0). Post-injection medications included 0.2 mg Buprenorphine (*s.c.*, for analgesia during the first day), 5 mg/kg Enrofloxacin as antibiotic and 0.3 mg/kg BW Meloxicam for anti-inflammatory purposes for 10 days. The eyes were followed clinically for 49 days after implantation was performed. The microrobots were manipulated (i.e., rotated and moved a maximum distance of their body length) at 28 days after implantation and the effect of robot manipulation was observed. F3

The condition of the eyes was examined for inflammatory-response related changes (see Supplementary material: Protocol for ophthalmic examination pre and postimplantation of intravitreal steerable inserts). Slit lamp biomicroscopy of the anterior segment using a hand-held slit lamp (Kowa SL-15) with 10/16× magnification was used. Indirect ophthalmoscopy of the posterior segment (i.e., vitreous, retina, and optic nerve) was performed using a Heine Omega 200 indirect ophthalmoscope and 20, 30, and 40 diopter condensing lenses. Tonometry was used to determine intraocular pressure (IOP) using a calibrated rebound tonometer (TonoVet). A modified McDonald-Shadduck[27] score system (see Supplementary material: Ocular irritation scoring scale based on modified McDonald-Shadduck score system) was used to grade inflammatory changes in the anterior and posterior segment. Ophthalmic examinations were carried out as described above when the animals arrived at the research facility, as well as

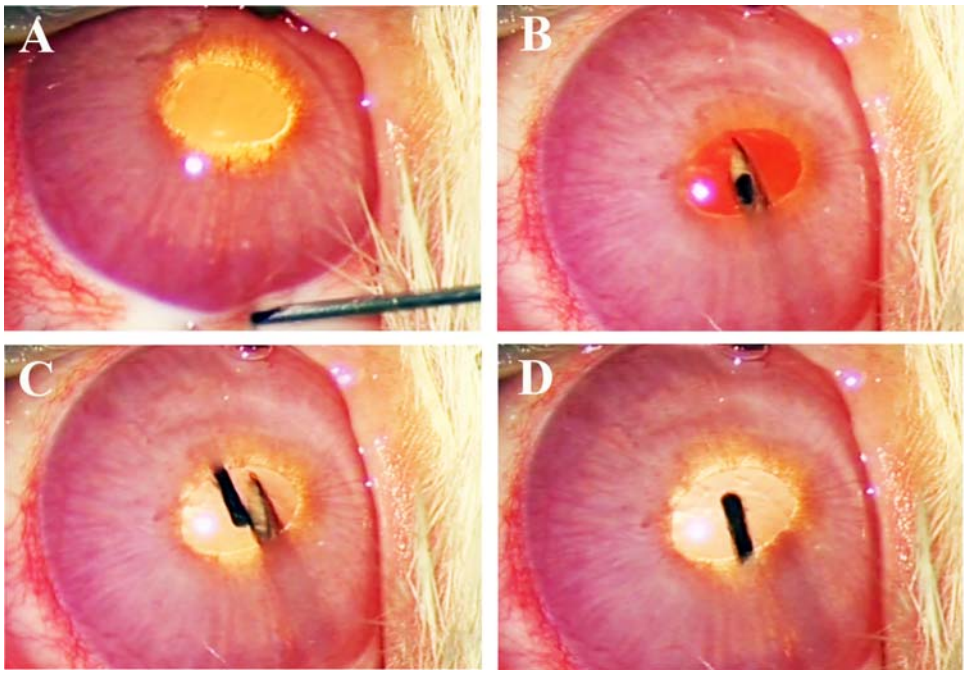

COLOR

FIGURE 3. **A**: Pars plana injection with 23G needle placement 1 mm peripheral to the internal limbus. A precise needle placement is required to prevent damage to adjacent tissues. **B**: Visualization of the needle position within the vitreous cavity through the pupil. **C**: Ejection of a microrobot from the needle tip: 0.1 mL of HA was used to push the microrobot out of the needle tip. **D**: Successful placement of a microrobot in the center of the vitreous after retraction of the needle.

one day prior to the planned intervention with the microrobot implantation or sham injections. Follow-up examinations were organized every day during the first three days after the injection, and subsequently, once every week until euthanasia (day 50). Immediately after euthanasia the eyes were surgically removed and placed in a modified Karnovsky's fixative (Paraformaldehyde 2%, Glutaraldehyde 2.5% in 0.1*M* Sodium Phosphate buffer) for 24 h at room temperature. The eyes were then placed in a 0.1*M* NaP buffer solution for shipment to the Comparative Ophthalmic Pathology Laboratory of Wisconsin (University of Wisconsin-Madison) where the eyes were examined histopathologically by light microscopy.

Data were evaluated using descriptive statistics. No statistical comparisons were performed since calculations with noncontinuous longitudinal datasets require a relatively high number of subjects for adequate power. This was not the case, nor the objective in this study.

The Zurich cantonal Swiss Veterinary Office approved all the protocols used (i.e., treatment, monitoring, animal housing) based on the Swiss decree on animal protection. The protocols are in accordance with the principles and policies in the Animal Welfare Act and NIHGuide for Care and Use of Laboratory Animals.

RESULTS

This section presents the results from the corrosion tests, fibroblast cell tests, and *in in v*ivo rabbit experiments performed to explore biocompatibility and suitability of the microrobots for implantation.

Corrosion tests

Figure 4 shows typical potentiodynamic polarization curves for coated and uncoated microrobots. Table II presents statistics on corrosion potential E_{corr} and corrosion current density j_{corr} determined by Tafel analysis. The corrosion potential *E*corr of Ppy-coated microrobots was significantly higher than that of Au coated (type I) or uncoated microrobots (p-values $< 3.7 \cdot 10^{-2}$), which indicates a more "noble" nature of the surface reacting with HBSS. Also, *E*corr for Au coating type II was significantly higher than that of the uncoated (p values $= 3.5 \cdot 10^{-2}$). However, the difference between *E*corr of Au coating type I and II (p values $= 6.3 \cdot 10^{-1}$) was statistically insignificant at 95% confidence level. All microrobots had minimal j_{corr} (i.e., the j_{corr} values were <3 μA·cm^{-2}; the mean j_{corr} values were <2 μA·cm^{-2}). The j_{corr} values indicated that

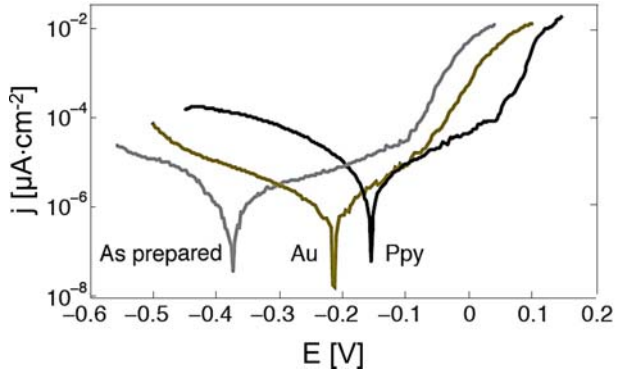

COLOR

FIGURE 4. Tafel plots of the microrobots tested in HBSS medium: uncoated CoNi surface (as prepared), electrodeposited Au surface (Au), and electrodeposited Ppy surface (Ppy).

TABLE II. Mean and SD Values of E_{corr} and j_{corr} Measured from the Microrobots.

	Corrosion Potential E_{corr} (mV)		Rate of Corrosion j_{corr} ($\mu A\ cm^{-2}$)	
Microrobot Types	Mean	SD	Mean	SD
Uncoated ($N = 5$)	−327	58	1.46	0.15
Au type I ($N = 6$)	−264	81	1.92	0.77
Au type II ($N = 5$)	−214	56	1.12	0.50
Ppy ($N = 3$)	−145	6	(*)	(*)

there was a lesser release of ions from Au coating type II than from uncoated microrobots. *NB*: Ppy is a conducting polymer, hence current measured (i.e., corresponding current density $4.83 \pm 0.76\ \mu A \cdot cm^{-2}$) is a sum of corrosion currents and doping/undoping currents between the microrobot and the HBSS [see (*) in Table II].

The surface of the microrobots was analyzed by SEM following the potentiodynamic polarization tests. All the microrobots preserved their integrity [Figure 5(A)], although some localized features were observed. In particular, a microcracked surface was noticed for the Ppy-coated microrobots [Figure 5(D)]. The cracks typically occur due to the Ppy doping process.[23] Na, Ca, Cl, O, and P elements originating from the HBSS solution residue [see Figure 5(B)] were typically detected in the corresponding EDX patterns (data not shown). Despite the aforementioned features, the surface of the microrobots did not show any traces of Co and Ni, as proven by XPS analyses (Supporting Information Figure S2). Hence, the Au coatings completely sealed the CoNi body from direct contact with HBSS medium. Indeed, the survey spectrum of the Ppy-coated microtubes was very similar to that of the as-prepared material.[23] C and O were the main elements detected by XPS at the uttermost surface in both Au (type I and type II)- and Ppy-coated microtubes. Additionally, N was detected in the latter. Na, Ca, and P were detected in small amounts in the Au-coated microtubes by XPS as well. These were likely coming from the HBSS solution. The oxygen content in the uncoated microrobots was found to be low (<4 wt %) by EDX, indicating that the CoNi alloy did not oxidize extensively. Actually, the Co/Ni ratio remained the same in both uncoated and coated robots (38 at% Co, 62 at% Ni). This indicates that no preferential release of Co or Ni ions took place in the former despite the absence of any protective coating.

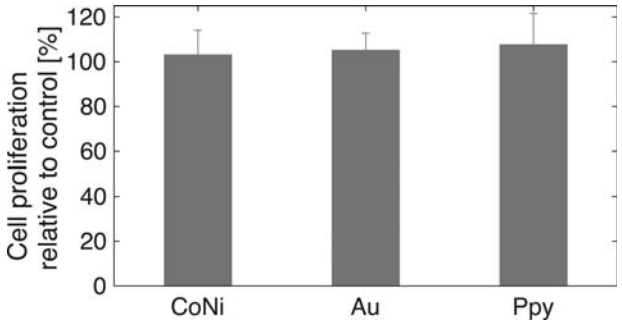

FIGURE 6. Mean values of cell proliferation relative to control with SDs in error bars ($n > 4$ samples for each microrobot type; 7 as-prepared microrobots with a CoNi surface, 4 Au-coated type II microrobots, and 8 Ppy-coated microrobots). 100% corresponds to the mean proliferation of the cells in the PBS solvent referred to as control (four control samples).

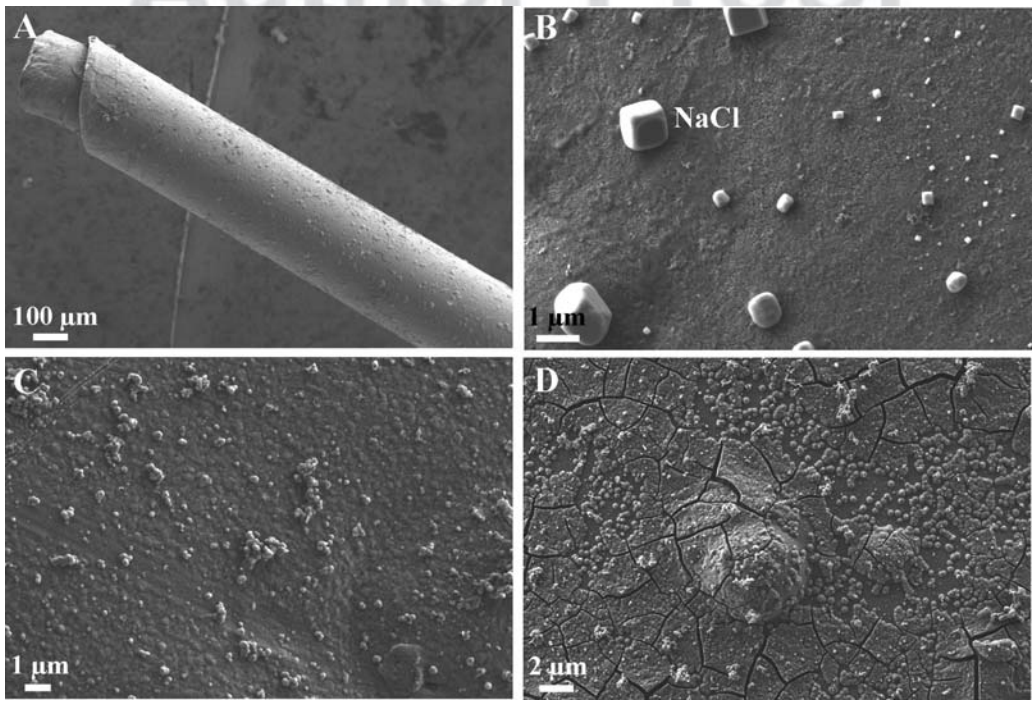

FIGURE 5. The SEM images shown were taken after the corrosion tests of a Au (type I) coated CoNi microrobot, shown in **A**. The zoomed details of the external surface for uncoated (**B**), Au (type I) coated (**C**), and Ppy/Au-coated (**D**) microrobots.

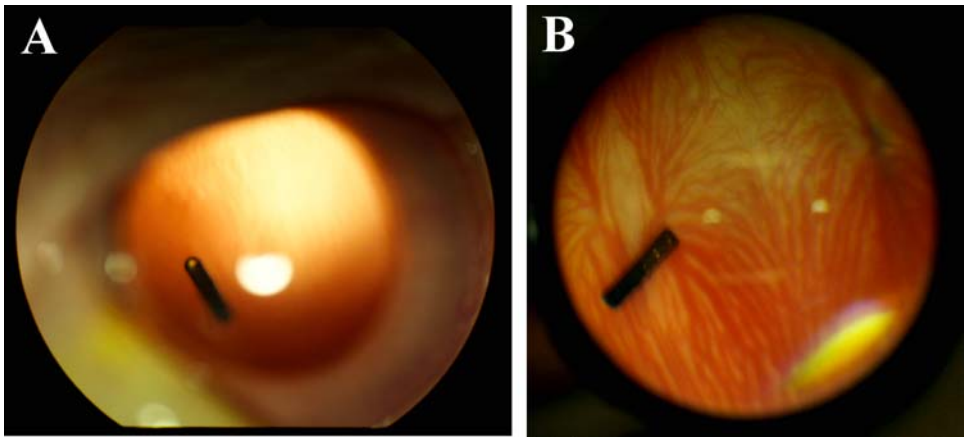

COLOR

FIGURE 7. Two typical images from the rabbit eyes one day after injection. **A**: A microrobot placed in the central part of the vitreous. **B**: A microrobot placed in the posterior part of the vitreous adjacent to the retina.

In vitro fibroblast viability

NIH3T3 fibroblast viability was determined by tetrazolium conversion that monitors the mitochondrial activity as an indication of living cells. Cell proliferation relative to control (Figure 6) was indistinguishable for uncoated microrobots, coated microrobots, and the control samples. The positive viability data gained from the *in vitro* cell culture assay were the motivation to perform *in vivo* biocompatibility trials in living rabbit eyes.

F6

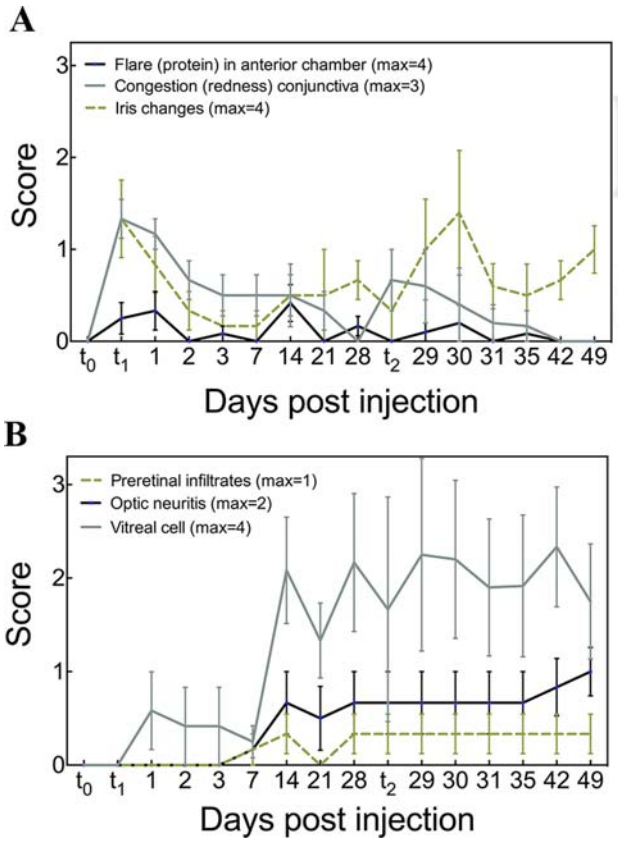

COLOR

FIGURE 8. Inflammatory changes observed in microrobot-implanted rabbit eyes ($n = 6$). **A**: General inflammatory changes in the anterior segment of the eye. **B**: Inflammatory changes in the posterior segment of the eye. The time point t_0 is baseline, t_1 indicates 4 h after microrobot injection, and t_2 indicates 4 h after microrobot manipulation. Remark: "max = 1–4" refers to the maximal clinical scores assigned to the various clinical variables that were scored according to the "Ocular irritation scoring scale based on modified McDonald-Shadduck score system (Altmann et al.[27]), which is provided in Suporting Information.

In vivo rabbit experiments

A Ppy-coated microrobot was injected with 0.1 mL HA into the ocular posterior segment (vitreous) of one randomly assigned eye in six healthy female New Zealand white rabbits (Group A1) (Figure 7). Six more rabbits received a sham injection of 0.1 mL HA alone (Group B1). The posterior lens capsule was inadvertently damaged during the injection procedure in the first two eyes receiving a microrobot (Group A1) and in the first two eyes receiving a sham injection (Group B1). As a direct result of the lens capsule laceration a focal cataract developed in all of these four eyes. Only minimal inflammatory changes that are potentially related to the lens capsule ruptures were observed clinically and histopathologically. No study-related clinical or histopathologic abnormalities were observed in any of the fellow eyes not receiving injections (Groups A0 and B0). Clinically, eyes receiving HA sham injections (Group B1)

F7

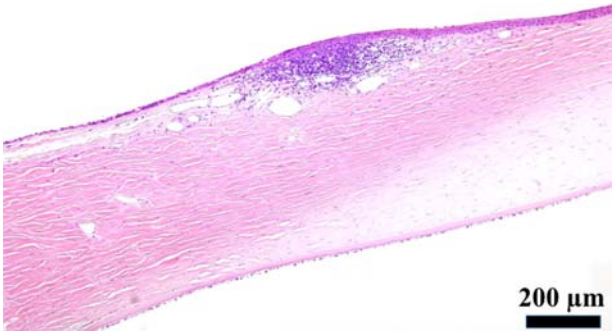

COLOR

FIGURE 9. Mild limbal lymphoplasmacytic episcleritis in the vicinity of the injection site observed in all eyes receiving sham injections. This is a sign of very mild, local injection procedure-related inflammation in these eyes. Hematoxylin and eosin (H&E) histopathology stain (Image courtesy R.R.Dubielzig, COPLOW).

COLOR

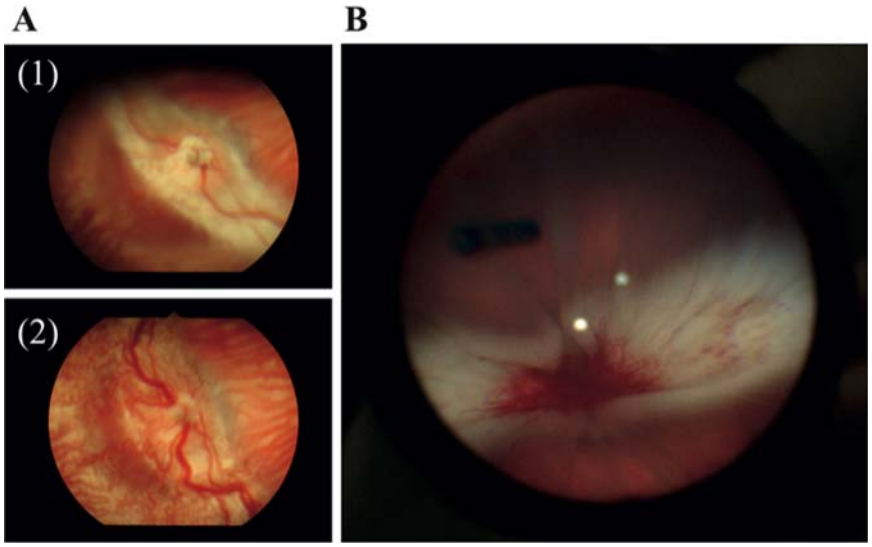

FIGURE 10. **A**: (1) Baseline examination one day prior to microrobot injection. (2) Optic neuritis ($n = 1$) at 14 days post microrobot injection in the same eye as (1). Note the dilation of pre-existing blood vessels on and around the optic nerve head compared to the situation in the same eye at the baseline examination. **B**: Complete retinal detachment and optic neuritis at 28 days post microrobot injection. Blood vessel dilation and formation of new blood vessels are visible at the location of the optic nerve head. The detached retina can be observed as folded membranous structure that originates at the optic nerve head and fans out toward the periphery. The injected microrobot is visible at the top left side of the image.

COLOR

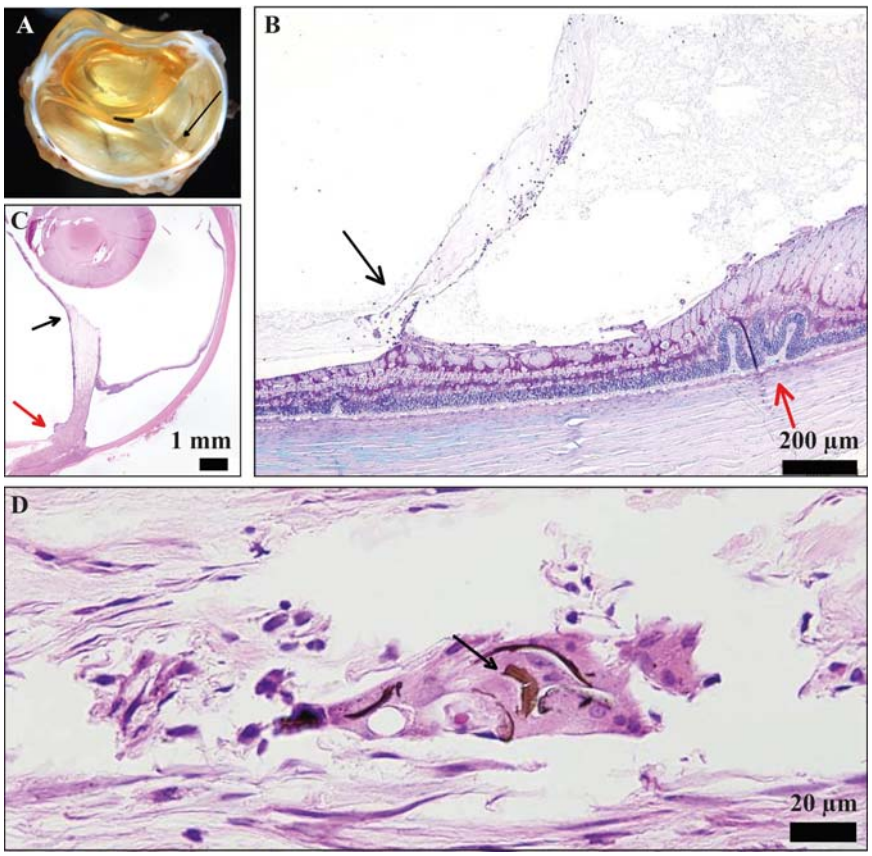

FIGURE 11. All images demonstrate histopathologic changes in eyes post microrobot injection (Images courtesy R.R.Dubielzig, COPLOW). **A**: Macroscopic image of a hemisected eye with a microrobot (black linear object) embedded in the vitreous behind the lens. The lens is yellow as a result of the fixative used to prepare the eye for histopathology. A vitreal traction band extends from the retina toward the microrobot (black arrow). **B**: Complete retinal detachment (black arrow). The optic nerve head is indicated by the red arrow. The ocular lens is visible as oval structure at the top of the image. H&E histopathology stain. This is the same eye as in Figure 10(B). **C**: A vitreal traction band (black arrow) at its point of attachment to the retina below. Retinal folds are visible on the right side of this image (red arrow). Periodic acid–Schiff (PAS) histopathology stain. **D**: Brown foreign material (black arrow), potentially Ppy coating, in a multinucleated giant cell. This is the same eye as in Supporting Information Figure S4(C). (H&E histopathology stain).

showed mild inflammatory changes, which subsided within the first 2 weeks after injection (Figures 8). Histopathology revealed a minimal limbal lymphoplasmacytic episcleritis in the vicinity of the injection site, which is a sign of very mild, local injection procedure related inflammation in these eyes (Figure 9).

During the first week after injection, eyes receiving microrobots (Group A1) exhibited mild inflammatory changes [Figure 8(A, B)] similar to those observed in the eyes receiving HA sham injections [Figures S3(A-C) in Supplementary material]. The changes in the anterior part of the eye predominated and were interpreted to be a result of the injection procedure rather than the HA, since HA is a natural part of the vitreous. Inflammatory changes in the posterior segment of five out of six eyes receiving microrobots appreared (preretinal cell infiltrates and optic neuritis) or significantly increased (vitreal cells) during the second week after microrobot implantation [Figure 8(B) and Supporting Information Figure S3(C)]. One eye had an optic nerve inflammation [Figure 10(A)]. A second eye had a complete and permanent detachment of the retina [Figure 10(B)]. These two eyes were unresponsive to light. A partial retinal detachment occurred in four more eyes, which was temporary in three eyes and permanent for the study duration in one. A tear or hole in the retina was observed clinically in two eyes. Such ocular changes were not observed in any of the control groups [Supporting Information Figure S3(C)]. No obvious obvious surface changes were observed opthalmoscopically on the microrobots prior to euthanasia [Supporting Information Figure S4(A, B)], apart from a small flake of detached Ppy coating could be observed on one of the microrobots [Supporting Information Figure S4(C)].

By the end of the follow-up, histopathologic studies confirmed that the inflammation was accompanied by the presence of vitreous traction bands ($n = 3$) [Figure 11(A)], retinal wrinkling/folding ($n = 3$) [Figure 11(B)], retinal tear ($n = 2$), retinal detachment ($n = 2$) [Figure 11(C)], retinal atrophy ($n = 3$), or optic neuritis ($n = 1$). Histopathologic sections also demonstrated multinucleated giant cells with phagocytosed brown foreign material in one of the rabbit eyes [Figure 11(D)], corresponding to the eye demonstrated in Supporting Information Figure S4(C)]. The microrobot manipulation did not cause a significant increase of inflammatory changes apart from increased scores for conjunctival congestion and iris changes detected during the three following days [Figure 8(A) and Supporting Information Figure S3(A-B)]. However, the level of inflammation in the vitreous had already reached a significant level by that time [Figure 8(B) and Supporting Information Figure S3(C)].

DISCUSSION

Steerable ophthalmic microrobots are envisioned in ocular applications that require implantation. Coated (Au and Ppy) and uncoated (as-prepared CoNi) microrobots were investigated for their corrosion properties and for cell viability. The corrosion current density values as measured by potentiodynamic polarization were minimal (i.e., $j_{corr} < 3\ \mu A \cdot cm^{-2}$ for uncoated and Au coated; *ND*: current density of Ppy $< 5.5\ \mu A \cdot cm^{-2}$ includes doping/undoping currents). The corrosion potentials showed a trend consistent with the intrinsic nobility of the materials. Also, galvanic pairs between the CoNi alloy and the nobler Au layer that could cause severe oxidation of the CoNi material in the coated microrobots were not observed. This result suggests that Au (type I and II layers) homogeneously coats the CoNi alloy surface and exerts some sealing effect [Figure 5(C)].

NIH3T3 fibroblasts cultured in solution, in which coated or uncoated microrobots were stored for 7 days, were viable and proliferated normally. This finding indicates that no cytotoxic compounds were released from the microrobots into the supernatant after 7 days in solution. This result is consistent with the low corrosion current densities determined by electrochemical corrosion analyses.

In vivo tests with implantation in rabbit eyes were performed using Ppy-coated implants. The presence of significant inflammatory responses after the second week following injection can be interpreted to demonstrate the unsuitability of the microrobots for long-term implantation. A cracked Ppy surface [Figure 5(D)] used to enhance antibiofouling properties,[23] enlarges the surface area in ocular contact, and therefore increases the risk of releasing potentially harmful sulfonate ions stabilized within the Ppy structure. Also, the presence of phagocytosed brown foreign material within multinucleated giant cells in one of the rabbit eyes could indicate an inflammatory reaction to released Ppy [Figure 11(D)], even though the Ppy has exhibited biocompatibility on surface.[23] Rabbit eyes have been found among the most sensitive *in vivo* models,[28,29] which could explain the severity of the responses observed. The absence of significant inflammatory responses during the entire first week following injection motivates to continue investigating coated microrobots for implantation. Whether the uninflamed state of the eyes can be preserved with timely removal of the microrobots needs to be confirmed in an implantation—explantation study setup. A careful *in vivo* biocompatibility characterization should be carried out if Ppy is intended for an ophthalmic application. The presented results provide valuable information for those who work on implant technology and biocompatibility. The future capability for microrobot implantation can realize the potential to enable a new generation of surgical,[5,8,9] targeted drug delivery[4,9,11,12] and diagnostic[7] techniques involving implantation in the posterior segment of the eye.

ACKNOWLEDGMENTS

Kartik Sivaraman is acknowledged for his contribution to the literature search. We would also like to acknowledge Tonci Novkovic for contributing in preparation of the CAD illustrations. Bumjin Jang is acknowledged for helping with preparing Au coating type II. Manuela Eugster is acknowledged for her work on Labview interface for the control of corrosion tests. Dr Richard Dubielzig at the Comparative Ophthalmic Pathology Laboratory of Wisconsin is acknowledged for providing ocular histopathology evaluation. E. Pellicer is grateful to Spanish MINECO for the "Ramon y Cajal" contract (RYC-2012-10839). E.P. and J.S. acknowledge 2014-SGR-1015 from Generalitat de Catalunya.

REFERENCES

1. Friedman DS, O'Colmain BJ, Munoz B, Tomany SC, McCarty C, De Jong PT, Nemesure B, Mitchell P, Kempen J. Prevalence of age-related macular degeneration in the United States. Arch Ophthalmol 2004;122:564–572.
2. Saaddine JB, Honeycutt AA, Narayan KV, Zhang X, Klein R, Boyle JP. Projection of diabetic retinopathy and other major eye diseases among people with diabetes mellitus. Arch Opthalmol 2008;126:1740–1747.
3. Ohji M, Tano Y. New instruments in vitrectomy. In: Kirchhof B, Wong D, editors. Vitreo-Retinal Surgery. New York: Springer; 2007. pp 85–98.
4. Kummer MP, Abbott JJ, Kratochvil BE, Borer R, Sengul A, Nelson BJ. OctoMag: an electromagnetic system for 5-DOF wireless micromanipulation. IEEE Trans Robot 2010;26:1006–1017.
5. Ullrich F, Bergeles C, Pokki J, Ergeneman O, Erni S, Chatzipirpiridis G, Pané S, Framme C, and Nelson BJ. Mobility experiments with microrobots for minimally invasive intraocular surgery. Invest Ophthalmol Vis Sci 2013;54:2853–2863.
6. Nelson BJ, Kaliakatsos IK, Abbott JJ. Microrobots for minimally invasive medicine. Annu Rev Biomed Eng 2010;12:55–85.
7. Ergeneman O, Chatzipirpiridis G, Pokki J, Toro MM, Sotiriou, Medina-Rodrígez S, Sánchez JF, Fernandéz-Gutiérrez A, Pané S, Nelson BJ. *In vitro* oxygen sensing using intraocular microrobots. IEEE Trans Biomed Eng 2012;3104–3109.
8. Ergeneman O, Pokki J, Počepcová V, Hall H, Abbott JJ, Nelson BJ. Characterization of puncture forces for retinal vein cannulation. J Med Device 2011;5:0445041–0445046.
9. Chatzipirpiridis G, Ergeneman O, Pokki J, Ullrich F, Fusco S, Ortega JA, Sivaraman KM, Nelson BJ, Pané S. Electroforming of implantable tubular magnetic microrobots for wireless ophthalmologic applications. Adv Healthc Mater 2014;4:209–214.
10. Pokki J, Ergeneman O, Sevim S, Enzmann V, Torun H, Nelson BJ. Measuring localized viscoelasticity of the vitreous body using intraocular microprobes. Biomed Microdevices. Forthcoming.
11. Fusco S, Chatzipirpiridis G, Sivaraman K, Ergeneman O, Nelson BJ, and Pané S. Chitosan electrodeposition for microrobotics drug delivery. Adv Healthc Mater 2013;2:1037–1044.
12. Pokki J, Ergeneman O, Sivaraman K, Özkale B, Zeeshan MA, Lühmann T, Nelson BJ, Pané S. Electroplated porous polypyrrole nanostructures patterned by colloidal lithography for drug-delivery applications. Nanoscale 2012;4:3083–3088.
13. Lloyd AW, Faranger RG, and Denyer SP. Ocular biomaterials and implants. Biomaterials 2001;22:769–785.
14. Brunette DM, editor. Titanium in medicine: material science, surface science, engineering, biological responses, and medical applications. New York: Springer; 2001.
15. Olson JL, Velez-Montoya R, Erlanger M. Ocular biocompatibility of nitinol intraocular clips. Invest Ophthalmol Vis Sci 2012;53:354–360.
16. Gerding H, Taneri S, Benner FP, Thelen U, Uhlig CE, and Reichelt R. Successful long-term evaluation of intraocular titanium tacks for the mechanical stabilization of posterior segment ocular implants. Materwiss Werksttech 2001;32:903–912.
17. Demann E, Stein P, Haubenreich J. Gold as an implant in medicine and dentistry. J Long Term Eff Med Implants 2005;15:687–698.
18. Hughes OH. Incorporating gold into ocular prosthetics. J Ophthal Prosthet 2010. AQ3
19. Querques G, Cascavilla ML, Cavallero E, Triolo G, Querques L, Lattanzio R, Cicinelli MV, Preziosa C, Borrelli E, Bandello F. Changes in macular function after Ozurdex for retinal vein occlusion. Optom Vis Sci 2014;91:760–768.
20. Arcinue CA, Cerón OM, Foster CS. A comparison between the fluocinolone acetonide (Retisert) and dexamethasone (Ozurdex) intravitreal implants in uveitis. J Ocul Pharmacol Ther 2013;29: 501–507.
21. Meleth AD,Wong WT, and Chew EY. Treatment for atrophic macular degeneration. Curr Opin Ophthalmol 2011;22:190–193.
22. George PM, Lyckman AW, LaVan DA, Hegde A, Leung Y, Avasare R, Testa C, Alexander PM, Langer R, Sur M. Fabrication and biocompatibility of polypyrrole implants suitable for neural prosthetics. Biomaterials 2005;26:3511–3519.
23. Sivaraman KM, Özkale B, Ergeneman O, Lühmann T, Fortunato G, Zeeshan MA, Nelson BJ, and Pané S. Redox Cycling for passive modification of polypyrrole surface properties: effects on cell adhesion and proliferation. Adv Healthc Mater 2013;2:591–598.
24. Chiou GCY, Xuan B, and Rohde B. *In vi*tro methods in ophthalmic toxicology. Chiou GVY, editor. Ophthalmic Toxicology. Ann Arbor: CRC Press; 1999.
25. Jang B, Pellicer E, Guerrero M, Chen X, Choi H, Nelson BJ, Sort J, and Pané S. Fabrication of segmented Au/Co/Au nanowires: insights in the quality of Co/Au Junctions. ACS Appl Mater Interfaces 2014;6:14583–14589.
26. Epstein SP, Ahdoot M, Marcus E, Asbell PA. Comparative toxicity of preservatives on immortalized corneal and conjunctival epithelial cells. J Ocul Pharmacol Ther 2009;25:113–119.
27. Altmann S, Emanuel A, Toomey M, McIntyre K, Covert J, Dubielzig RR, Leatherberry G, Murphy CJ, Kodihalli S, Brandt CR. A quantitative rabbit model of vaccinia keratitis. Invest Ophthalmol Vis Sci 2010;51:4531–4540.
28. Bito LZ. Species differences in the responses of the eye to irritation and trauma: a hypothesis of divergence in ocular defense mechanisms, and the choice of experimental animals for eye research. Exp Eye Res 1984;39:807–829.
29. Chiou GCY. Ophthalmic toxicology. CRC Press, 1999. AQ4

AQ1: Please check whether short title is OK as typeset.

AQ2: Please check whether grant information is OK as typeset.

AQ3: Please provide volume number and page range for Ref. 18.

AQ4: Please provide publisher location for Ref. 29.

AQ5: Please confirm that given names (red) and surnames/family names (green) have been identified correctly.